

Coastal vulnerability mapping of the fjords in the Romsdal area, Norway using geoinformatics

Michail Giannakoudakis, George P. Petropoulos*, Spyridon E. Detsikas

Department of Geography, Harokopio University of Athens, Greece

*Correspondence: gpetropoulos@hua.gr

1. Introduction

In the light of climate change, it has become of critical importance to monitor Critical Water Zones (Bianchi et al., 2020). Among these zones, fjords, as geomorphological features located mainly at high latitudes, require special attention. Fjords have a distinct transverse and long profile, referred to as a U-shape (*Encyclopedia of geomorphology*, 2004). In these geomorphs, solid precipitation makes its way to the sea by eroding the bed and, as it flows, creates a rocky channel, much like liquid precipitation in temperate countries. In those formations, erosion rates are variant, characterized by low rates at the highest levels of the formations ranging from 0.2 to 1 mm per, as opposed to the lower levels where it increases significantly, on the order of 1 cm per year.

The importance of fjords is undeniable great both for the areas surrounding them and for the wider areas indirectly affected by them. These glacier-engraved features further represent the transition from terrestrial to marine environments and typically include sediments that highlight climatic and environmental changes over time (Howe et al., 2010)). Furthermore, it is well documented that submarine mass movements occur frequently in fjords and may be associated with a wide range of movement mechanisms. Mass transfer deposits (MTDs) associated with such processes may account for more than 70% of fjord basin fills (Bellwald et al., 2016). However, as mass movements have been identified over time periods characterized by changing sedimentation rates, sediment supply alone cannot explain the observed mass movement clusters (Schultze et al., 2022). Given the dynamic nature of those formations and their importance for climate and local communities, it has become of critical importance to adopt labor and cost-efficient method to assess manmade or natural changes imposed on this habitat.

To this end, Earth Observation (EO) technologies pose as an ideal solution. Satellite missions, especially multi-spectral missions, are the most common source of data for land cover classification due to their high temporal resolution and suitability for efficient computer processing (Radočaj et al., 2020). Amongst the existing EO programs, Landsat mission is considered one of the most important with over 50 years archive (Arévalo et al., 2023), allowing quantification of impacts, while providing the information necessary to understand long-term consequences and understanding the long-term evolution of fjords (Wulder et al., 2022). The results of continuous fjord monitoring can form the basis for formulating policies and regulations for appropriate protection and development of the resources and specificity of the region, and for planning the development of local industry.

A particularly promising methodology in evaluating the vulnerability of Arctic coasts is a multivariate geospatial index, the so-called Coastal Vulnerability Index (CVI). CVI expresses the degree of vulnerability of a coastline by taking into consideration different physical factors such as geomorphology, oceanographic factors (sea level rise, wave height, and tidal range), and shoreline retreat or advance to estimate the degree of vulnerability of a coastal area. Coupling CVI with advanced geoinformation tools (Tsatsaris et al., 2021), including EO imagery, unmanned aerial vehicles that enable data collection from a safe distance. Classifying the observed area into several generalized land cover categories creates a universal basis for spatial planning and monitoring changes in the environment (Faust et al., 2017). This index is important for identifying coastal segments and infrastructures as well

45 as other activities that are essentially susceptible to the risk posed by different physical factors
46 (Kovaleva et al., 2022). CVI has been extensively applied to various environmental settings, but its
47 application in the Arctic is yet underexplored with only a limited number of studies existing (Jaskólski et
48 al., 2017; Toumasi et al., 2024).

49 The present study aims to assess the coastal vulnerability of a fjord system located in Norway using
50 geoinformatics. This case study highlights the application of advanced technologies in understanding
51 and managing coastal dynamics, particularly in the context of climate change. By leveraging geospatial
52 tools and datasets, the research provides insights into the risks faced by Arctic coastal regions, offering
53 valuable information for sustainable management and adaptation strategies.

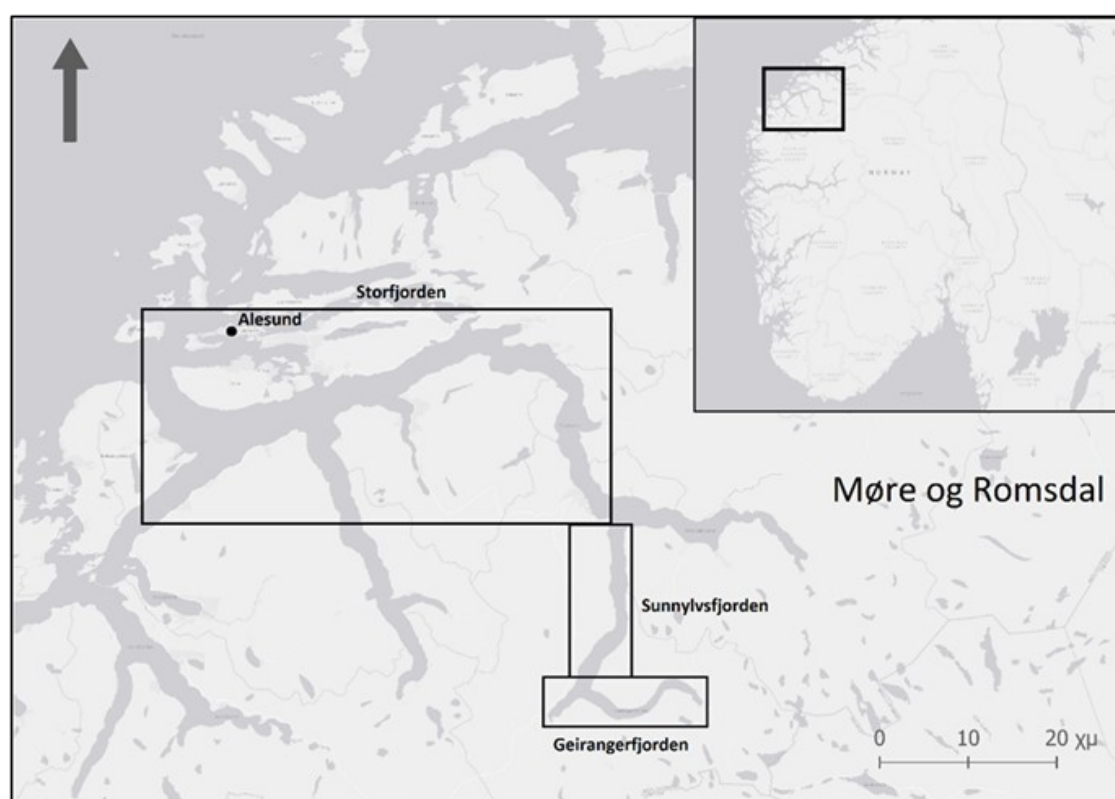
54 2. Experimental set-up

55

56 2.1. Study Area

57 As the experimental site of this case study, a fjord located in western Norway, in Møre og Romsdal
58 County (Møre og Romsda) has been selected. Norway has a total area of 385,207 square kilometres and
59 a population of 5,425,270 inhabitants (Eurostat, 2022). The country has a long eastern border with
60 Sweden and also shares borders with Finland, Russia and Denmark. Norway has an extensive coastline,
61 in the North Atlantic Ocean and the Barents Sea. The examined county is consisted of three districts of
62 Sunnmøre, Romsdal and Nordmøre, and with population close to 266 thousand people, according to the
63 latest census of 2022 ("Eurostat," n.d.). To better organize the study area will be divided into three
64 different points (Figure 1). These consist of the main branch of the system, which is Storfjorden and
65 connects the coastal area and by extension the sea to the mainland. It then moves on to the secondary
66 branch, in which Storfjorden, Sunnlyvsfjorden and finally ends in Geirangerfjorden. These three parts
67 are of interest both for the physical and anthropo-geographical features that define the whole.

68



69

70 **Figure 1:** The geographical location of the examined fjord system. The experimental site is split into
71 three sub-districts the Storfjorden, Sunnlyvsfjorden and Geirangerfjorden.

72 2.2. Datasets

73 CVI consists of a multivariate index that considers several factors that can influence the vulnerability
74 degree. For the purposes of this study, six variables linked to natural characteristics and physical
75 processes (geomorphology, slope, shoreline change, oceanographic conditions) were considered in
76 reflecting the coastal vulnerability of the study area. Below, an analytical description of each variable
77 used for the estimation of CVI is presented. Different analysis systems were therefore used to retrieve
78 these data, and thus different tools were used to produce results.

79 2.2.1. Geospatial data

80 Satellite data from Landsat sensor were collected by the USGS are
81 LC09_L2SP_201016_20220920_20230328_02_T1 and the similar framing data for the year 2022. The
82 LT05_L2SP_201016_20100927_20200823_02_T1 and its counterparts for the year 2010. The latest for
83 satellite data is the LT05_L2SP_201016_20000307_20200907_02_T2 for the year 2000. Initially, the date
84 chosen is September, a period when there is no significant cloud cover in the available image and even
85 more importantly in the area of interest. At the same time, the percentage that was set as the cloud cover
86 threshold is 10%, which limits images that are likely to have clouds over the fjord and prevent the smooth
87 process of preparing the paper. In addition, Copernicus Digital Elevation Model (European Space Agency
88 (2024)., n.d.), which provides elevation information at 30m spatial resolution, was selected to determine
89 the geomorphs DEM and slope rate of the coastal area.

90 2.2.2. Oceanographic data

91 Regarding the representation of the oceanographic conditions of the area, three parameters were taken
92 into consideration during the CVI estimation. Those consist of (i) the relative sea level change of the
93 examined area expressed in units of millimeters per year (mm/yr), (ii) the mean tide range expressed in
94 meters, and (iii) the mean wave height conditions expressed also in meters. Data about the relative sea
95 level rise and mean tidal range between 2010 and 2020 were obtained by a tide gauge station installed
96 near Alesund, available through the Norwegian Hydrographic Services Mapping Authority database
97 (api.sehavniva.no, accessed on 10 October 2024). The data recorded by the tidal gauge was considered
98 representative for the whole examined area. Regarding mean wave height, a value of 1.0 m was selected
99 based on the physiographical characteristics of the wider area and in accordance with other similar
100 studies which took place in the wider geographical area. In combination with the wave height, equally
101 important is the isostasy that characterises the area and alters the influence of the wave height. This
102 isostasy, according to the model "NKG2016LU_abs" and the website containing the wave data
103 (Kartverket), is at 2.1 mm. Regarding, mean sea level the resulting values were -1.2 cm for 2010 and 4.7
104 cm for 2020. Considering the isostasy from the model "NKG2016LU_abs", 2.1 mm are subtracted from
105 these values.

106 3. Methodology

107 3.1. Data pre-processing

108 Prior to estimating coastal vulnerability, following data acquisition, it is imperative to prepare the data
109 through pre-processing to ensure its usefulness for producing reliable results. All processing steps
110 implemented herein were performed using ENVI 5.3 software.

111 3.1.1. Geomorphology

112
113 The process of the project starts with the transfer of the DEM data from OpenTopography in the GIS
114 program. In parallel, to further validate the geomorphs produced by the DEM classification, high
115 resolution stereo imagery was used through ("Norge i Bilder," n.d.) (<https://norgeibilder.no/>). By

116 observing the area in 3D, it was possible to validate the DEM-derived geomorphs and make adjustments
 117 where needed.

118 3.1.2. Shorelines accretion/erosion rates

119 To estimate shoreline accretion and erosion rates, the coast from the two Landsat images were extracted
 120 using a binary supervised classification. Spectral signatures from land and water were recorded, and
 121 raster-to-vector conversion was performed on the classified images using ENVI 5.3 software to extract
 122 the shorelines of the study area.

123 The Maximum Likelihood Classification (MLC) method was identified as the most suitable for performing
 124 the binary classification. Statistically robust, this method is grounded in Bayes' theorem, which
 125 calculates marginal distributions and internal correlations under the assumption of multivariate
 126 normality in N-dimensional Euclidean space (Gevana et al., 2015). The classification accuracy was
 127 validated using metrics such as overall accuracy and Cohen's Kappa coefficient. The results
 128 demonstrated a high degree of reliability, with an overall accuracy of 99.65% and a Kappa coefficient of
 129 0.99, confirming the method's effectiveness in evaluating satellite imagery.

130 Subsequently, after extracting the coastline from the classified imagery using standard GIS procedures,
 131 the Digital Shoreline Analysis System (DSAS) tool was employed to calculate the shoreline displacement
 132 rate. DSAS, an Esri ArcGIS extension developed by the United States Geological Survey (USGS), enables
 133 the calculation of shoreline change rates using shorelines from different dates. This tool has significantly
 134 advanced shoreline change analysis globally. DSAS generates cross sections, or transects,
 135 perpendicular to a user-defined baseline along the coast. These transects are modelled from a
 136 theoretical baseline located at a set distance from the most recent shoreline. The tool then calculates
 137 the intersection points of each shoreline with the cross sections, enabling the computation of shoreline
 138 change rates (Sunny et al., 2022).

139 3.3 Estimating Coastal Vulnerability Index

140 After pre-processing the CVI factors into the appropriate format, the vulnerability degree of each factor
 141 was classified into 5 categories using the ranking suggested by (Jaskólski et al., 2017) which is being
 142 presented into Table 1.

143 **Table 1.** The Coastal Vulnerability Index (CVI) ranks variables into five categories, each representing a
 144 different level of vulnerability, ranging from very low to very high as suggested by (Jaskólski et al., 2017)

Vulnerability Ranking	Very Low	Low	Moderate	High	Very High
Parameter	1	2	3	4	5
Geomorphology	Rocky, cliffed coast, fjords, fiards	Medium cliffs, indented coasts	Low cliffs, glacial drift, alluvial plains	Cobble beaches, estuary	Barrier beaches, sand beaches, deltas, sand spits
Coastal slope (°)	>10.0	6.0–10.0	3.1–6.0	1.0–3.0	<1.0
Relative sea level change (mm/yr)	<1.8	1.8–2.5	2.5–2.95	2.95–3.16	>3.16
Shoreline erosion/accretion (m/yr)	>2.0	1.0–2.0	(–1.0)–(+1.0)	(–1.1)–(–2.0)	<–2.0
Mean tide range (m)	>6.0	4.1–6.0	2.0–4.0	1.0–1.9	<1.0
Mean wave height (m)	<0.55	0.55–0.85	0.85–1.05	1.05–1.25	>1.25

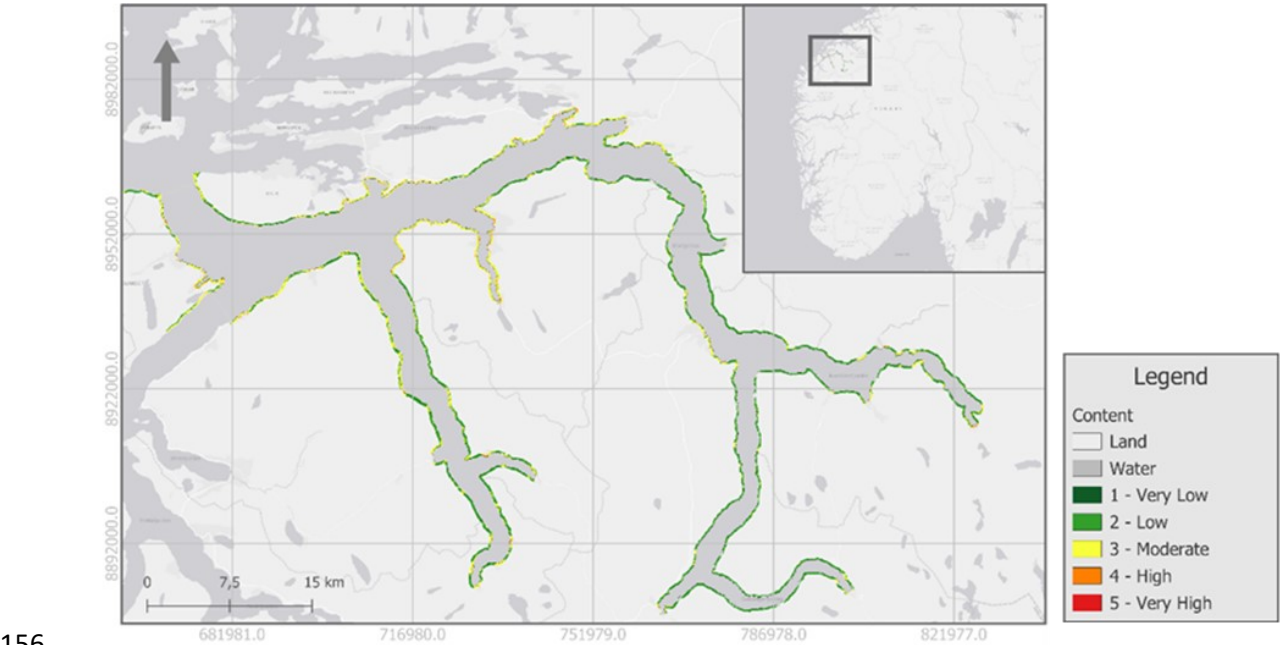
145 After assigning to each one of CVI parameters its vulnerability ranking, CVI was estimated using the
 146 following formula (equation 1):

147
$$CVI = \sqrt{\frac{a * b * c * d * e * f}{6}} \quad (equation\ 1)$$

148 where a = geomorphology, b = shoreline change rates, c = coastal slope, d = relative sea level rate, e =
 149 mean significant wave height, and f = mean tidal range.

150 **4. Results**

151 The resulted CVI map of the experimental site is presented in Figure 2. The resulted map showcased low
 152 to moderate risk throughout the examined area. Coast segments closer to the fiord entrance, belonging
 153 to the Storfjorden segment, showcased higher degrees of vulnerability. On the contrary, coasts that
 154 belong to the Sunnylvsfjorden and Geirangerfjorden segments depict in general a lower degree of
 155 vulnerability.



156
 157 **Figure 2:** The coastal vulnerability index map.

158
 159 The resulting graph shows that most of the study area is characterized by very low and low risk, which
 160 indicates the absence of changes in the places that make up these classes. Added to this is the moderate
 161 hazard, in which the parts that make up this class do not show significant alteration in their relief. Finally,
 162 the areas of high and very high risk make up only 8% of the area, indicating that there are areas that
 163 require observation and intervention in a few cases. From these results, it appears that the study area is
 164 mostly covered by areas that are not at immediate risk.

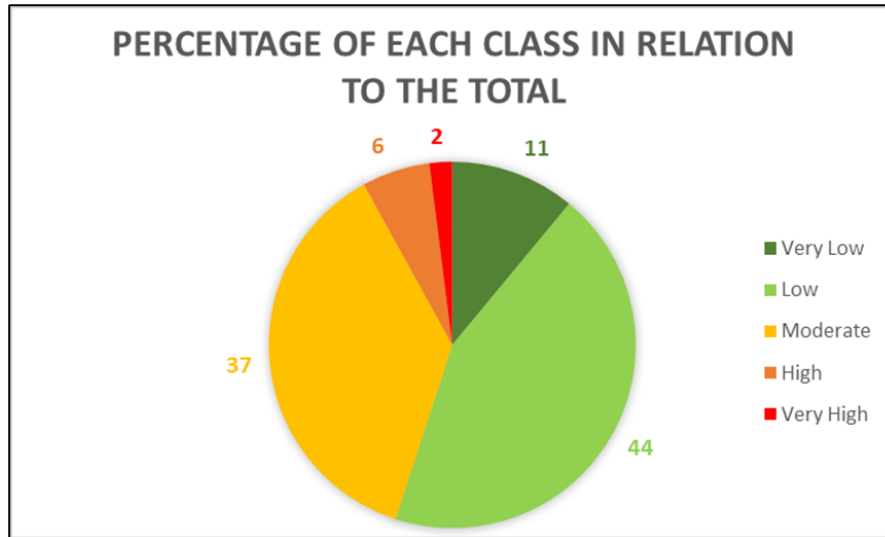


Figure 3: Graph for the percentage (%) of each class within the study area

In terms of each individual factor of CVI, the map resulting from the pre-processing and data processing presents a visualization of the geomorphological risk, dividing it into five classes in ascending order of hazard, from least to most dangerous. According to the generated image (Figure 4, a), most of the fjord system is characterized by low hazard (class 2), with the northern parts predominantly exhibiting moderate hazard (class 3). A few regions in the southern and eastern parts of the system are classified as very low hazard (class 1). By analyzing the image of the area (Figure 4, b), which has been broken into smaller sections for better interpretation, areas with high (class 4) to very high (class 5) coastal slope risk indices are identified. These high-risk areas are typically located in beach regions, where hollow formations transition towards lowland areas. Conversely, areas with minimal erosion exhibit indices ranging from very low to low, indicating a reduced coastal slope risk. These variations are associated with a very low risk level for the entire study area. Data obtained from DSAS were further simplified into a single set of values (Figure 4, d), highlighting considerable differences in shoreline variation hazards. Moderate risk values dominate, suggesting that the area has experienced several geomorphological changes over time. Comparing the mean tidal range with changes in sea surface height (Figure 4, c), both similarities and differences are evident. In terms of similarities, the values between points show minimal deviations, resulting in consistent visualization of data along the coastline. However, the mean tidal range exhibits exclusively high values, in contrast to the low relative sea level variations. Regarding wave dynamics, the mean wave height is limited to high hazard values, like the mean tidal range (Figure 4, e). These findings suggest that the fjord system operates largely autonomously from the open sea due to minimal internal variations, whereas the open sea demonstrates significant changes driven by weather conditions.

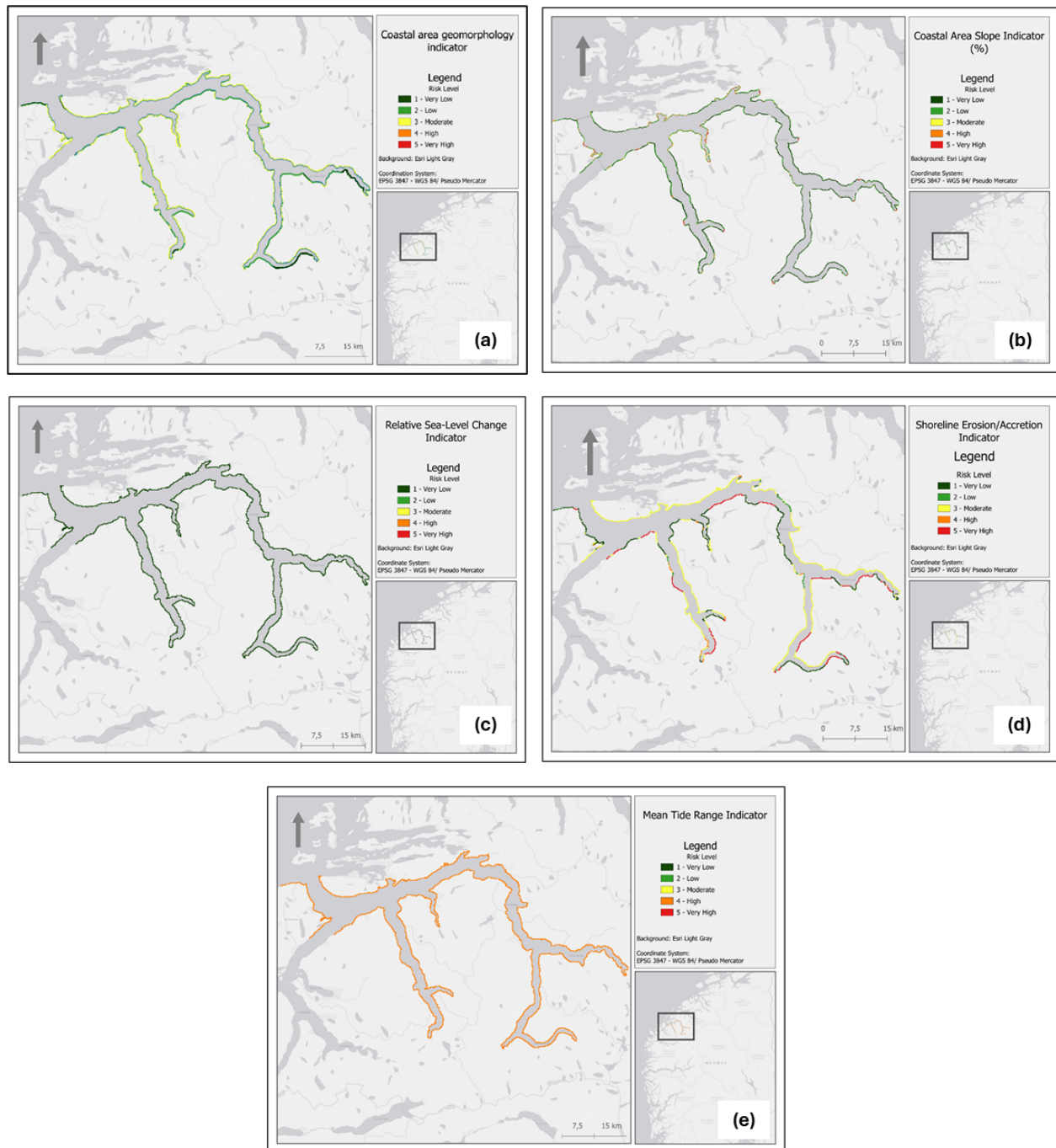


Figure 4. Maps depicting the vulnerability assessment of individual CVI (Coastal Vulnerability Index) factors: (a) Geomorphology ranking, (b) Coastal slope ranking, (c) Relative Sea level change ranking, (d) Shoreline erosion/accretion ranking, and (e) Mean tide range ranking. Red hues represent Very high and high degrees of vulnerability, yellow moderate degree of vulnerability and green hues Low and very low degree of vulnerability

5. Discussion

The objective of this study was to assess the vulnerability of a fjord system in Norway using the Coastal Vulnerability Index (CVI) in conjunction with geospatial datasets. The results indicate that the degree of coastal vulnerability in the studied area ranges from low to moderate. The analysis highlights that the most critical factors affecting CVI are relative sea level change and mean tide range, both contributing to very high vulnerability along the entire coastline. Following these, coastal slope and shoreline erosion/accretion are also significant, with high vulnerability observed in most parts of the coastline.

201 Mean wave height plays a moderate role, as evident in vulnerability patterns across the area. The factor
202 with the least influence is geomorphology, which indicates low vulnerability throughout the coastline,
203 consistent with findings from similar studies in similar experimental set-ups such as Finland and other
204 parts of Norway that attribute low vulnerability to the geological composition of the coastlines (Kovaleva
205 et al., 2022; Toumasi et al., 2024).

206 Results align with findings from other Arctic studies, such as those on Longyearbyen, Svalbard (Jaskólski
207 et al., 2017), where high vulnerability correlates with low coastal slope and limited sediment supply,
208 particularly in deltaic systems. Similarly, human interventions, such as the construction of artificial
209 coastlines, significantly influence CVI values, as observed in Longyearelva Delta. Comparative studies
210 from other regions, such as the Eastern Gulf of Finland and the Croatian coast of Istria, reveal moderate
211 to low coastal vulnerability (Kovaleva et al., 2022; Šimac et al., 2023). These findings underscore the
212 importance of regional geomorphological and climatic factors in determining coastal vulnerability.
213 Compared to the literature and sources with a similar focus, such as the studies by (Creel et al., 2022;
214 Hansen et al., 2007), the similarities that emerge are the alteration of the anaglyph and the variations in
215 the values of variables such as mean wave height.

216 A notable methodological limitation of this study arose from assigning equal weight to all factors in the
217 CVI calculation. This uniform weighting does not reflect real-world dynamics where certain factors, such
218 as relative sea level change and shoreline erosion, may have greater impacts. Future studies should
219 incorporate differential weighting to enhance accuracy. Furthermore, this research lays the groundwork
220 for integrating socio-economic indicators alongside physical geography to provide a more
221 comprehensive vulnerability assessment. The EO-PERSIST project, emphasizing socio-economic
222 studies in Arctic environments, offers a promising resource for addressing data gaps and developing
223 methodological approaches to integrate socioeconomic with geospatial datasets to assess coastal
224 vulnerability (Petropoulos et al., 2023). By addressing these challenges and leveraging robust databases,
225 like the one that EO-PERSIST aims to develop, future studies can refine CVI methodologies, ensuring
226 accurate assessments and informing sustainable management practices for vulnerable Arctic
227 coastlines.

228 **Final Remarks**

229 The aim of the study was to assess the coastal vulnerability of the fjords in the study area using
230 geoinformatics. By observing the results produced and analysing the individual elements and their
231 combination, it is possible to compare them with the initial hypotheses set. Geomorphology, coastline
232 and coastal vulnerability index contribute to this, creating the differences. As far as geomorphology is
233 concerned, it has a positive sign in its influence on the area, due to the low risk along the entire length of
234 the area. Similarly, the coastline is characterised for the most part by low risk, with the exception of
235 certain parts where it is moderate or increased, which are worthy of observation. Finally, the coastal
236 vulnerability index shows mixed results, with the predominant ones being moderate and low risk. In
237 terms of the problems encountered, the first is the reduced list of satellite imagery near the poles,
238 specifically in the earlier time periods. The second is the little information on the waters, which may be
239 due to the limited number of tide gauges in the area.

240 Following the progress and development of the work, a future direction is to combine this information
241 with the anthropogeographic data, so that the work has a practical application. A continuation of this is
242 more targeted research as a reference to the distribution of this population within the urban fabric, which
243 areas need more attention depending on the size of the population and the type of problem that plagues
244 each area. At the same time, one issue that can be taken into account is human intervention in the area
245 and how it has shaped the landscape over the years. Finally, an equally important addition to the above
246 is research into how glaciers affect the coastline and submarine relief during the winter period. By
247 combining all of the above suggestions with the results of this work, a comprehensive CVI model can be
248 created. This, can be applied to any region regardless of the prevailing geographical and political
249 conditions, making it suitable for any region of the world. Still, a more targeted analysis of the current

250 study area would be to calculate the future shape of the study area's relief, with the aim of preventing
251 disasters and taking advantage of opportunities that may arise.

252 **Acknowledgments**

253 The present research study has been financially supported by the project “EO-PERSIST”, funded by
254 European Union’s Horizon Europe Research and Innovation program HORIZON-MSCA-2021-SE-01-01
255 under grant agreement N. 101086386. Thanks also to Dr. Konstantinos Tsanakas and Dr. Antigoni Faka
256 for their valuable feedback during the preparation of this research work.

257 **References**

- 258 Arévalo, P., Baccini, A., Woodcock, C.E., Olofsson, P., Walker, W.S., 2023. Continuous mapping of
259 aboveground biomass using Landsat time series. *Remote Sensing of Environment* 288, 113483.
260 <https://doi.org/10.1016/j.rse.2023.113483>
- 261 Bellwald, B., Hjelstuen, B.O., Sejrup, H.P., Haflidason, H., 2016. Postglacial mass movements and
262 depositional environments in a high-latitude fjord system – Hardangerfjorden, Western Norway.
263 *Marine Geology* 379, 157–175. <https://doi.org/10.1016/j.margeo.2016.06.002>
- 264 Bianchi, T.S., Arndt, S., Austin, W.E.N., Benn, D.I., Bertrand, S., Cui, X., Faust, J.C., Koziorowska-Makuch,
265 K., Moy, C.M., Savage, C., Smeaton, C., Smith, R.W., Syvitski, J., 2020. Fjords as Aquatic Critical
266 Zones (ACZs). *Earth-Science Reviews* 203, 103145.
267 <https://doi.org/10.1016/j.earscirev.2020.103145>
- 268 Creel, R.C., Austermann, J., Khan, N.S., D’Andrea, W.J., Balascio, N., Dyer, B., Ashe, E., Menke, W., 2022.
269 Postglacial relative sea level change in Norway. *Quaternary Science Reviews* 282, 107422.
270 <https://doi.org/10.1016/j.quascirev.2022.107422>
- 271 Encyclopedia of geomorphology, 2004. . London ; New York : Routledge.
- 272 European Space Agency (2024)., n.d. Copernicus Global Digital Elevation Model.
273 <https://doi.org/10.5069/G9028PQB>.
- 274 Eurostat [WWW Document], n.d. URL <https://ec.europa.eu/eurostat/en/> (accessed 12.6.24).
- 275 Faust, J.C., Scheiber, T., Fabian, K., Vogt, C., Knies, J., 2017. Geochemical characterisation of northern
276 Norwegian fjord surface sediments: A baseline for further paleo-environmental investigations.
277 *Continental Shelf Research* 148, 104–115. <https://doi.org/10.1016/j.csr.2017.08.015>
- 278 Gevana, D., Camacho, L., Carandang, A., Camacho, S., Im, S., 2015. Land use characterization and
279 change detection of a small mangrove area in Banacon Island, Bohol, Philippines using a
280 maximum likelihood classification method. *Forest Science and Technology* 11, 197–205.
281 <https://doi.org/10.1080/21580103.2014.996611>
- 282 Hansen, L., Eilertsen, R.S., Solberg, I.-L., Sveian, H., Rokoengen, K., 2007. Facies characteristics,
283 morphology and depositional models of clay-slide deposits in terraced fjord valleys, Norway.
284 *Sedimentary Geology* 202, 710–729. <https://doi.org/10.1016/j.sedgeo.2007.08.004>
- 285 Howe, J.A., Austin, W.E.N., Forwick, M., Paetzel, M., Harland, R., Cage, A.G., 2010. Fjord systems and
286 archives: a review, in: Howe, J. A., Austin, W. E. N., Forwick, M., Paetzel, M. (Eds.), *Fjord Systems*
287 *and Archives*. Geological Society of London, p. 0. <https://doi.org/10.1144/SP344.2>
- 288 Jaskólski, M., Pawłowski, Ł., Strzelecki, M., 2017. Assessment of geohazards and coastal change in
289 abandoned Arctic town, Pyramiden, Svalbard. pp. 41–49.
- 290 Kovaleva, O., Sergeev, A., Ryabchuk, D., 2022. Coastal vulnerability index as a tool for current state
291 assessment and anthropogenic activity planning for the Eastern Gulf of Finland coastal zone (the
292 Baltic Sea). *Applied Geography* 143, 102710. <https://doi.org/10.1016/j.apgeog.2022.102710>
- 293 Norge i Bilder [WWW Document], n.d. URL <https://norgeibilder.no/> (accessed 12.10.24).
- 294 Petropoulos, G.P., Karathanassi, V., Sandric, I., Sykas, D., Scholtze, M., Kubowicz, Ł., Carpio, G.D.,
295 Lemmetyinen, J., Chersich, M., Krischke, M., Detsikas, S.E., 2023. EO-PERSIST: a Cloud-based
296 Remote Sensing Data System for Promoting Research and Socioeconomic Studies in Arctic
297 Environments. <https://doi.org/10.5281/zenodo.8143140>

298 Radočaj, D., Obhodaš, J., Jurišić, M., Gašparović, M., 2020. Global Open Data Remote Sensing Satellite
 299 Missions for Land Monitoring and Conservation: A Review. *Land* 9, 402.
 300 <https://doi.org/10.3390/land9110402>
 301 Schultze, S., Andersen, T., Hessen, D.O., Ruus, A., Borgå, K., Poste, A.E., 2022. Land-cover, climate and
 302 fjord morphology drive differences in organic matter and nutrient dynamics in two contrasting
 303 northern river-fjord systems. *Estuarine, Coastal and Shelf Science* 270, 107831.
 304 <https://doi.org/10.1016/j.ecss.2022.107831>
 305 Šimac, Z., Lončar, N., Faivre, S., 2023. Overview of Coastal Vulnerability Indices with Reference to
 306 Physical Characteristics of the Croatian Coast of Istria. *Hydrology* 10, 14.
 307 <https://doi.org/10.3390/hydrology10010014>
 308 Sunny, D.S., Islam, K.M.A., Mullick, Md.R.A., Ellis, J.T., 2022. Performance study of imageries from
 309 MODIS, Landsat 8 and Sentinel-2 on measuring shoreline change at a regional scale. *Remote*
 310 *Sensing Applications: Society and Environment* 28, 100816.
 311 <https://doi.org/10.1016/j.rsase.2022.100816>
 312 Toumasi, P., Petropoulos, G.P., Detsikas, S.E., Kalogeropoulos, K., Tselos, N.G., 2024. Coastal
 313 Vulnerability Impact Assessment under Climate Change in the Arctic Coasts of Tromsø, Norway.
 314 *Earth* 5, 640–653. <https://doi.org/10.3390/earth5040033>
 315 Tsatsaris, A., Kalogeropoulos, K., Stathopoulos, N., Louka, P., Tsanakas, K., Tsesmelis, D.E.,
 316 Krassanakis, V., Petropoulos, G.P., Pappas, V., Chalkias, C., 2021. Geoinformation Technologies
 317 in Support of Environmental Hazards Monitoring under Climate Change: An Extensive Review.
 318 *ISPRS International Journal of Geo-Information* 10, 94. <https://doi.org/10.3390/ijgi10020094>
 319 Wulder, M.A., Roy, D.P., Radeloff, V.C., Loveland, T.R., Anderson, M.C., Johnson, D.M., Healey, S., Zhu,
 320 Z., Scambos, T.A., Pahlevan, N., Hansen, M., Gorelick, N., Crawford, C.J., Masek, J.G.,
 321 Hermosilla, T., White, J.C., Belward, A.S., Schaaf, C., Woodcock, C.E., Huntington, J.L.,
 322 Lymburner, L., Hostert, P., Gao, F., Lyapustin, A., Pekel, J.-F., Strobl, P., Cook, B.D., 2022. Fifty
 323 years of Landsat science and impacts. *Remote Sensing of Environment* 280, 113195.
 324 <https://doi.org/10.1016/j.rse.2022.113195>
 325